Available online at www.sciencedirect.com
ScienceDirect
International Journal of Heat and Mass Transfer 50 (2007) 2986–2995
International Journal of HEAT and MASS TRANSFER
www.elsevier.com/locate/ijhmt

Interfacial area concentration in annular two-phase flow

Tatsuya Hazuku [a,*], Tomoji Takamasa [a], Takashi Hibiki [b], Mamoru Ishii [b]

[a] *Faculty of Marine Technology, Tokyo University of Marine Science and Technology, Koto, Tokyo 135-8533, Japan*
[b] *School of Nuclear Engineering, Purdue University, 400 Central Drive, West Lafayette, IN 47907-2017, USA*

Received 28 September 2005; received in revised form 11 December 2006
Available online 29 March 2007

Abstract

Accurate prediction of the interfacial area concentration is essential to successful development of the interfacial transfer terms in the two-fluid model. The interfacial area concentration in annular flow and annular-mist flow is especially relevant to the transition process to the liquid film dryout, which might lead to fatal problem in the safety and efficient operation of boiling heat transfer system. However, very few experimental and theoretical studies focusing on the interfacial area concentration in annular flow region have been conducted. From this point of view, measurements of annular flow parameters such as one-dimensional interfacial area concentration of liquid film and local interfacial area concentration profile of liquid film were performed by a laser focus displacement meter at 21 axial locations in vertical upward annular two-phase flow using a 3-m-long and 11-mm-diameter pipe. The axial distances from the inlet (z) normalized by the pipe diameter (D) varied over $z/D = 50$–250. Data were collected for preset gas and liquid flow conditions and for Reynolds numbers ranging from 31,800 to 98,300 for the gas phase and 1050 to 9430 for the liquid phase. Axial development of the one-dimensional interfacial area concentration and the non-dimensional local interfacial area concentration profile of liquid film were examined with the data obtained in the experiment. Total interfacial area concentration including liquid film and droplets was also discussed with help of the existing drift-flux model, entrainment correlation, and droplet size correlation.

Keywords: Interfacial area transport equation; Interfacial area concentration; Annular two-phase flow; Liquid film; Droplet; Laser focus displacement meter

1. Introduction

For many energy plants, annular-mist two-phase flow is the most common flow pattern in boiling heat transfer systems, such as boiler and heat exchanger. The flow characteristics of liquid film and entrained droplets in the annular-mist flow, especially the wave phenomena on a liquid film, play important roles in heat and mass transfer. The phenomena are closely related to the transition process to liquid film dryout, which might lead to fatal problems in plant safety and efficient operation. Accurate knowledge of the interfacial structure of liquid film in annular-mist flow is thus essential for proper thermal–hydraulics design and safety analysis of the plants.

The interfacial structure of liquid film and fraction of entrained droplet in annular-mist flow change continuously with flow development in the axial direction, because the axial changes of the pressure or the interfacial shear stress are very large compared with those of other flow patterns. Two-fluid model, which is applied to thermal–hydraulic analysis code for nuclear reactor, is considered as the most useful and practical model to predict such flow development in two-phase systems. However, in order to close the two-fluid model, the interfacial transfer terms should be modeled accurately. In the present thermal–hydraulic analysis codes, the effects of interfacial structure on the system behavior have been analyzed by using flow regimes and transition criteria. In this approach, no time or length scale is incorporated in calculating a developing flow. To solve such a problem, the introduction of interfacial area transport equation has been recommended [1]. The interfacial

* Corresponding author. Tel.: +81 3 5245 7727; fax: +81 3 5245 7410.
E-mail address: hazuku@kaiyodai.ac.jp (T. Hazuku).

0017-9310/$ - see front matter © 2007 Elsevier Ltd. All rights reserved.
doi:10.1016/j.ijheatmasstransfer.2007.01.017

Nomenclature

A	total cross-sectional area
A_d	cross-sectional area of droplets
A_f	liquid-film cross-sectional area
a_i	interfacial area concentration
$\tilde{a}_i$	non-dimensional interfacial area concentration ($\equiv a_i \Delta x$)
$a_{i,drop}$	interfacial area concentration of liquid droplets
$a_{i,film}$	interfacial area concentration of liquid film
C_{an}	roughness parameter of liquid film interface
D	pipe diameter
E	fraction of liquid flux flowing as droplet ($\equiv j_{fe}/j_f$)
E_d	fraction of liquid entrained in the gas core from total liquid area
E_∞	equilibrium value of fraction entrained, E
g	gravitational acceleration
j	mixture volumetric flux
j_c	total volumetric flux based on the gas-core area
j_f	superficial liquid velocity
j_{fe}	volumetric flux of liquid droplets
j_g	superficial gas velocity
$N_{\mu f}$	viscous number $[\equiv \mu_f/(\rho_f \sigma \sqrt{\sigma/g\Delta\rho})^{1/2}]$
R	pipe radius
Re_f	Reynolds number of liquid phase ($\equiv \langle j_f \rangle D/v_f$)
Re_g	Reynolds number of gas phase ($\equiv \langle j_g \rangle D/v_g$)
r	radial coordinate
r_d	droplet radius
r_{vm}	volume median radius
r_{Sm}	Sauter mean radius
t	time
v_{fc}	liquid–droplet velocity
v_{ff}	liquid-film velocity
v_{gc}	gas-core velocity
V_{gj}	drift velocity
We	entrainment Weber number $[\equiv \rho_g \langle j_g \rangle^2 D (\Delta\rho/\rho_g)^{1/3}/\sigma]$
z	axial coordinate

Greek symbols

α	void fraction
α_c	fraction of gas core
α_d	droplet fraction in the gas core
δ	liquid-film thickness
$\overline{\delta}$	time-averaged liquid film thickness
Γ	volumetric flow rate per unit wetted perimeter
η	interfacial area concentration of liquid film normalized by total interfacial area concentration ($\equiv \langle a_{i,film} \rangle / \langle a_{i,total} \rangle$)
μ_f	viscosity of liquid phase
μ_g	viscosity of gas phase
v_f	kinematic viscosity of liquid phase
v_g	kinematic viscosity of gas phase
ρ_f	liquid density
ρ_g	gas density
$\Delta\rho$	density difference between liquid and gas
σ	interfacial tension
ζ	dimensionless distance

Mathematical symbols

$\langle\ \rangle$	area-averaged quantity
$\langle\langle\ \rangle\rangle$	void fraction weighted cross-sectional area-averaged quantity

area transport equation can replace the traditional flow regime maps and regime transition criteria. The changes in the two-phase flow structure are predicted mechanistically by introducing the interfacial area transport equation. A successful development of the interfacial area transport equation thus can make a quantum improvement in the two-fluid model formulation.

Recently, continuous efforts have been made to develop the interfacial area transport equation particularly in dispersed two-phase flows [2–6]. However, very few experimental and theoretical studies focusing on the interfacial area transport in annular-mist flow have been conducted. In order to develop the accurate model on interfacial area transport equation in annular-mist flow, reliable experimental data on local flow characteristics such as liquid film and entrained droplet are required. As the first step in this direction, this study aims at measuring the detailed axial development of flow parameters such as one-dimensional interfacial area concentration of liquid film, and local interfacial area concentration profile of liquid film. The obtained one-dimensional interfacial area concentration of the liquid film is compared with the existing drift-flux model [7], and the contribution of the interfacial area concentration in the liquid film to total interfacial area concentration is estimated with help of existing drift-flux model [7], entrainment correlation [8], and droplet size correlation [9].

2. Preliminary modeling of interfacial area transport of annular two-phase flow

2.1. Drift-flux model in annular-mist flow

2.1.1. Gas-drift velocity of annular flow without droplet entrainment

In annular two-phase flows, the relative motions between phases are governed by the interfacial geometry, the body-force field, and the interfacial momentum transfer. The constitutive equation for the gas-drift velocity in annular two-phase flows can be derived by taking into account those macroscopic effects of the structured two-phase flow. Assuming steady-state adiabatic two-phase

annular flow without droplet entrainment, Ishii derived the constitutive equation for the gas-drift velocity, $\overline{V_{gj}}$, from the momentum equations for gas and liquid phases as [7]

$$\overline{V_{gj}} \equiv \langle v_g \rangle - \langle j \rangle \simeq \frac{1-\langle\alpha\rangle}{\langle\alpha\rangle + \left\{\frac{1+75(1-\langle\alpha\rangle)}{\sqrt{\langle\alpha\rangle}}\frac{\rho_g}{\rho_f}\right\}^{1/2}} \left[\langle j\rangle + \sqrt{\frac{\Delta\rho g D(1-\langle\alpha\rangle)}{0.015\rho_f}}\right], \tag{1}$$

where v_g, j, α, ρ_g, ρ_f, $\Delta\rho$, g and D are the gas velocity, the mixture volumetric flux, the void fraction, the gas density, the liquid density, the density difference, the gravitational acceleration and the channel diameter, respectively. $\langle\rangle$ means the area-averaged quantity.

2.1.2. Inception criteria for droplet entrainment

As the gas velocity increases in the annular flow, the liquid entrainment from the film to the gas-core flow takes place. Ishii and Grolmes [10] carefully examined the existing experimental data for the inception of entrainment in co-current two-phase flow systems, by plotting them on the liquid film Reynolds number, Re_f, versus the critical gas velocity plane, which indicates that there exist at least three different regimes for each fluid as shown in Fig. 1. Here, the liquid film Reynolds number is defined by

$$Re_f \equiv \frac{4\rho_f\langle\langle v_f\rangle\rangle\delta}{\mu_f} = \frac{4\Gamma}{v_f} = \frac{\langle j_f\rangle D}{v_f}, \tag{2}$$

where v_f, δ, μ_f, Γ, ν_f and j_f are the liquid velocity, the liquid film thickness, the liquid viscosity, the volumetric flow rate per unit wetted perimeter, the kinematic viscosity and the superficial liquid velocity, respectively. $\langle\langle\rangle\rangle$ means the void-fraction weighted mean quantity. The Reynolds number at the point A is roughly found to be 1635 [10].

Ishii and Grolmes derived the criteria for an onset of entrainment based on the balance of the forces acting on the wave as [10]

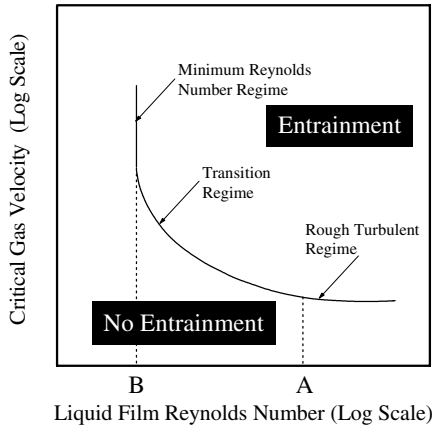

Fig. 1. Schematic inception boundary for a particular combination of liquid and gas [10].

$$\begin{cases} \frac{\mu_f\langle j_g\rangle}{\sigma}\sqrt{\frac{\rho_g}{\rho_f}} \geqslant 11.78 N_{\mu f}^{0.8} Re_f^{-1/3} & \text{for } N_{\mu f} \leqslant \frac{1}{15},\ Re_f \leqslant 1635, \\ \frac{\mu_f\langle j_g\rangle}{\sigma}\sqrt{\frac{\rho_g}{\rho_f}} \geqslant 1.35 Re_f^{-1/3} & \text{for } N_{\mu f} > \frac{1}{15},\ Re_f \leqslant 1635, \end{cases} \tag{3}$$

where j_g and σ are the superficial gas velocity and the surface tension, respectively. The liquid viscous number, $N_{\mu f}$, is defined by $\mu_f/[\rho_f\sigma\sqrt{\sigma/g\Delta\rho}]^{1/2}$. The inception criterion for the rough turbulent regime ($Re_f > 1635$) becomes

$$|j_g| > \frac{\sigma}{\mu_f}\sqrt{\frac{\rho_f}{\rho_g}} \times \begin{cases} N_{\mu f}^{0.8} & \text{for } N_{\mu f} \leqslant \frac{1}{15},\ Re_f > 1635, \\ 0.1146 & \text{for } N_{\mu f} > \frac{1}{15},\ Re_f > 1635. \end{cases} \tag{4}$$

However, in general, the gas flux is much larger than the liquid flux in the annular-mist flow regime; then, for a weakly viscous fluid such as water or sodium, Eq. (4) can be replaced by

$$|j_g| \simeq |j| > \left(\frac{\sigma\Delta\rho g}{\rho_g^2}\right)^{1/4} N_{\mu f}^{-0.2}. \tag{5}$$

If inequality (5) is satisfied, then the droplet entrainment into the gas-core flow should be considered; otherwise the correlation for annular flow, Eq. (1) can be applied [7].

2.1.3. Gas-drift velocity of annular-mist flow

The correlation for $\overline{V_{gj}}$ in annular-mist flows (annular flows without droplet entrainment) can be readily formulated by combining the drift-velocity constitutive equations for a dispersed flow and pure annular flow [7]. The area fraction of liquid entrained in the gas core from total liquid area at any cross section, E_d, is given by

$$E_d \equiv \frac{A_d}{A_f + A_d}. \tag{6}$$

Here, A_d and A_f are the cross-sectional area of droplets and the liquid-film cross-sectional area, respectively, see Fig. 2. The mean liquid–droplet fraction in the gas core alone, α_d, is given by

$$\alpha_d \equiv \frac{\text{cross-sectional area of drops}}{\text{cross-sectional area of core}} = \frac{A_d}{A - A_f} = \frac{(1-\langle\alpha\rangle)E_d}{\langle\alpha\rangle + (1-\langle\alpha\rangle)E_d}, \tag{7}$$

where A is the total cross-sectional area. The core-area fraction, α_c, is given by

$$\alpha_c \equiv \frac{\text{cross-sectional area of core}}{\text{total cross-sectional area}} = \frac{A - A_f}{A} = \langle\alpha\rangle + (1-\langle\alpha\rangle)E_d, \tag{8}$$

and the film-area fraction is given by $1 - \alpha_c$. By introducing the droplet area fraction in the gas core alone, α_d, the core-area fraction, α_c, is represented by

$$\alpha_c = \frac{\langle\alpha\rangle}{1-\alpha_d}. \tag{9}$$

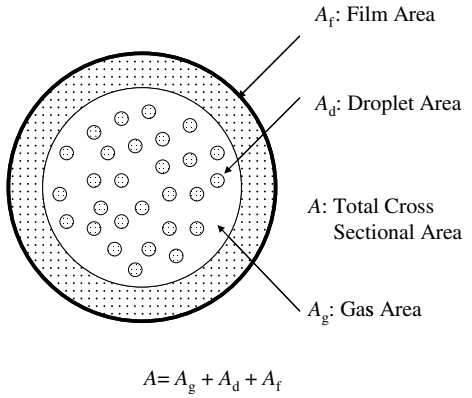

Fig. 2. Schematic cross-sectional diagram of annular-mist two-phase flow.

Consequently, α_c should be used in the annular flow correlation, Eq. (1), to obtain the relative motion between the core and the film, whereas α_d should be used in the dispersed-flow correlation to obtain a slip between droplets and gas-core flow.

By denoting the gas-core velocity, liquid–droplet velocity, and film velocity by v_{gc}, v_{fc} and v_{ff}, respectively, the total volumetric flux is given by

$$\langle j\rangle = [v_{gc}(1-\alpha_d) + \alpha_d v_{fc}]\alpha_c + v_{ff}(1-\alpha_c). \tag{10}$$

Furthermore, by denoting the total volumetric flux in the core, j_c, based on the core area by

$$j_c = v_{gc}(1-\alpha_d) + \alpha_d v_{fc}, \tag{11}$$

we have Eq. (12) from the annular correlation, Eq. (1),

$$j_c - \langle j\rangle \simeq \frac{1-\alpha_c}{\alpha_c + \left\{\frac{1+75(1-\alpha_c)}{\sqrt{\alpha_c}}\frac{\rho_g}{\rho_f}\right\}^{1/2}}\left[\langle j\rangle + \sqrt{\frac{\Delta\rho g D(1-\alpha_c)}{0.015\rho_f}}\right]. \tag{12}$$

It can be shown from the dispersed-flow correlation [7] and Eq. (11) that for a distorted-droplet or churn-droplet flow regime, the drift velocity can be given approximately by

$$\langle\langle v_g\rangle\rangle - j_c = \sqrt{2}\left(\frac{\sigma g\Delta\rho}{\rho_g^2}\right)^{1/4}\alpha_d. \tag{13}$$

Here we have used an approximation as $(1-\langle\alpha\rangle) \ll 1$. However, depending on the core-gas velocity, the dispersed-flow drift-velocity correlation for a much smaller particle should be used. When the droplets are generated by the entrainment of liquid film, the following approximate form is suggested for an undistorted-particle regime outside the Stokes regime [11] as

$$\langle\langle v_g\rangle\rangle - j_c = 0.5 r_d\left[\frac{(g\Delta\rho)^2}{\mu_g\rho_g}\right]^{1/3}\alpha_d, \tag{14}$$

where μ_g is the gas viscosity. Eq. (14) should be used when [7]

$$|\langle j\rangle| > 1.456\left(\frac{\sigma\Delta\rho g}{\rho_g^2}\right)^{-1/4}\left[\frac{\mu_g^2}{\rho_g\sigma\sqrt{\sigma/g\Delta\rho}}\right]^{-1/12}. \tag{15}$$

From Eqs. (12)–(14), we obtain

$$\overline{V_{gj}} = \frac{1-\alpha_c}{\alpha_c + \left\{\frac{1+75(1-\alpha_c)}{\sqrt{\alpha_c}}\frac{\rho_g}{\rho_f}\right\}^{1/2}}\left[\langle j\rangle + \sqrt{\frac{\Delta\rho g D(1-\alpha_c)}{0.015\rho_f}}\right] + \begin{cases}\sqrt{2}\left(\frac{\sigma g\Delta\rho}{\rho_g^2}\right)^{1/4}\alpha_d \\ \text{or} \\ \frac{r_d}{2}\left[\frac{(g\Delta\rho)^2}{\mu_g\rho_g}\right]^{1/3}\alpha_d.\end{cases} \tag{16}$$

If the radius of the particle is very small, then the essential contribution to the relative motion between phases comes from the first term of Eq. (16), and the core flow may be considered as a homogeneous dispersed flow. In such a case, Eq. (16) reduces to

$$\overline{V_{gj}} \simeq \frac{1-\alpha_c}{\alpha_c + \left\{\frac{1+75(1-\alpha_c)}{\sqrt{\alpha_c}}\frac{\rho_g}{\rho_f}\right\}^{1/2}}\left[\langle j\rangle + \sqrt{\frac{\Delta\rho g D(1-\alpha_c)}{0.015\rho_f}}\right]. \tag{17}$$

This expression shows a linear decrease of drift velocity in terms of entrained liquid fraction, which can be observed in various experimental data [12,13].

2.1.4. Droplet size

The droplet size and size distribution in annular-dispersed flow have been studied in detail by Kataoka et al. [9]. The radius in Eq. (16) is closely approximated by the volume median radius, r_{vm}, thus

$$r_d \simeq r_{vm} = 0.005\frac{\sigma}{\rho_g j_g^2}Re_g^{2/3}\left(\frac{\rho_g}{\rho_f}\right)^{-1/3}\left(\frac{\mu_g}{\mu_f}\right)^{2/3}, \tag{18}$$

where Re_g is the gas Reynolds number defined by $\rho_g\langle j_g\rangle D/\mu_g$.

2.2. Interfacial area concentration in annular-mist flow

The interfacial area in annular-mist flow is expressed as [14]

$$\langle a_i\rangle = \langle a_{i,film}\rangle + \langle a_{i,drop}\rangle = \frac{4C_{an}}{D}\sqrt{\frac{\langle\alpha\rangle}{1-\alpha_d}} + \frac{\langle\alpha\rangle}{1-\alpha_d}\left(\frac{3\alpha_d}{r_{Sm}}\right), \tag{19}$$

where C_{an} and r_{Sm} are the roughness parameter of liquid film and Sauter mean radius of droplets, respectively. The roughness parameter is the measure of the interfacial area increase due to waves on film, thus $C_{an} \geqslant 1$. In the following analysis, we assume axisymmetric liquid film thickness and axially smooth liquid film, namely $C_{an} = 1$. For $\langle\alpha\rangle \approx 1$ and $\alpha_d \ll 1$, Eq. (19) is further simplified to [14]

$$\langle a_i\rangle \simeq \frac{4}{D} + \frac{\langle\alpha\rangle}{1-\alpha_d}\left(\frac{3\alpha_d}{r_{Sm}}\right). \tag{20}$$

Sauter mean radius of droplets in annular-mist flow is related to the volume median radius by

$$r_{Sm} = 0.796 r_{vm}, \tag{21}$$

where the proportionality constant has been calculated from the droplet size distribution [9].

2.3. Fraction of liquid flux flowing as droplet in annular-mist flow

Assuming $C_{an} = 1$, the interfacial area concentration in annular-mist flow is calculated by Eq. (19) with α, α_d, and r_{Sm}. Sauter mean radius can be calculated by Eqs. (18) and (21), whereas void fraction is obtained by Eq. (16) with Eq. (18) and α_d. Thus, the key to estimate the interfacial area concentration in annular-mist flow is to obtain α_d.

In annular-mist flow, the droplet size is quite small and the gas flux is high, therefore the slip between droplets and gas is relatively small. Then, α_d may be approximated by [14]

$$\alpha_d \simeq E\frac{j_f}{j_g}, \tag{22}$$

where E is the fraction of liquid flux flowing as droplet defined as

$$E \equiv \frac{j_{fe}}{j_f}. \tag{23}$$

Here, j_{fe} is the volumetric flux of droplets. The fraction of liquid flux flowing as droplet can be calculated by Ishii and Mishima [8]

$$E = \left\{1 - \exp(-1.87 \times 10^{-5}\zeta^2)\right\}E_\infty, \tag{24}$$

where

$$\zeta = \frac{(z/D)Re_f^{0.5}}{We^{0.25}}, \tag{25}$$

$$E_\infty = \tanh(7.25 \times 10^{-7} We^{1.25} Re_f^{0.25}). \tag{26}$$

Here, Weber number is defined by

$$We \equiv \frac{\rho_g \langle j_g \rangle^2 D}{\sigma}\left(\frac{\Delta\rho}{\rho_g}\right)^{1/3}. \tag{27}$$

The averaged liquid film thickness is estimated from Eq. (9) as

$$\langle\delta\rangle = \frac{D}{2}\left(1 - \sqrt{\frac{\langle\alpha\rangle}{1-\alpha_d}}\right). \tag{28}$$

3. Experiment

Fig. 3 shows a two-phase flow loop used in the present experiments. The working fluids were air and water, which was obtained by purifying tap water to an electrical conductivity lower than 1 μS/cm. Air was fed into the channel from a compressor. The water was pumped from a water tank into a test pipe made of acrylic, passed through a flow meter, and flowed back to the water tank. A uniform liquid film was achieved by the use of a sintered metal pipe as a film generator. The inside diameter and length of the test pipe were 11 mm and 3 m, respectively. Water temperature was maintained at 25 ± 0.5 °C by a cooler submerged in the water tank. Thermocouples in the water tank and separation tank monitored the water temperature.

In this study, we performed the measurement of the microscopic interfacial wave structure of vertical annular two-phase flow using a laser focus displacement meter (LFD, Keyence Co. Japan, Model LT 8100). In the previous experiments conducted by Takamasa and his colleagues [15,16], interfacial waves on a film flowing down a vertical plate wall and down the inner wall of a pipe were measured using the LFD. The effectiveness of the LFD for obtaining detailed liquid film information was clarified through these studies. The LFD has a measurement range of 28 ± 1 mm from the laser head. The diameter of the beam spot is 2 μm, and the spatial resolution is 0.2 μm. The temporal resolution is approximately 1 kHz. Measurements of film thickness with the LFD were conducted at 21 axial locations, equally spaced 110 mm apart along the pipe axial length. The axial distance from the inlet (z) normalized by the pipe diameter (D) was $z/D = 50$–250. Data were collected for predetermined gas and liquid flow conditions and for Reynolds numbers ranging from $Re_g = 31{,}800$–$98{,}300$ for the gas phase and $Re_f = 1050$–9430 for the liquid phase.

4. Results and discussion

4.1. One-dimensional interfacial area concentration

Axial development of one-dimensional interfacial area concentration is examined in this section. In order to deduce the one-dimensional interfacial area concentration from measured local liquid film thickness, we assume axisymmetric interfacial wave. Then, one-dimensional interfacial area concentration of liquid film, $\langle a_{i,film}\rangle$, is estimated by taking the time-averaged liquid film thickness, $\overline{\delta}$, as follows:

$$\langle a_{i,film}\rangle = \frac{\sum a_{i,film}}{\sum t} = \frac{4(D - 2\overline{\delta})}{D^2}, \tag{29}$$

where $\overline{\delta} \equiv \sum \delta_i \Delta t_i / \sum \Delta t_i$. The axial development of the one-dimensional interfacial area concentration of liquid film is obtained by substituting the value of $\overline{\delta}$, measured at each axial location with the LFD, into Eq. (29). Comparison of the present experimental data with the data predicted by the interfacial area concentration model for annular-mist flow, which is taking into account the one-dimensional drift-flux model and the liquid entrainment model (refer to Eqs. (19) and (22)), is also examined.

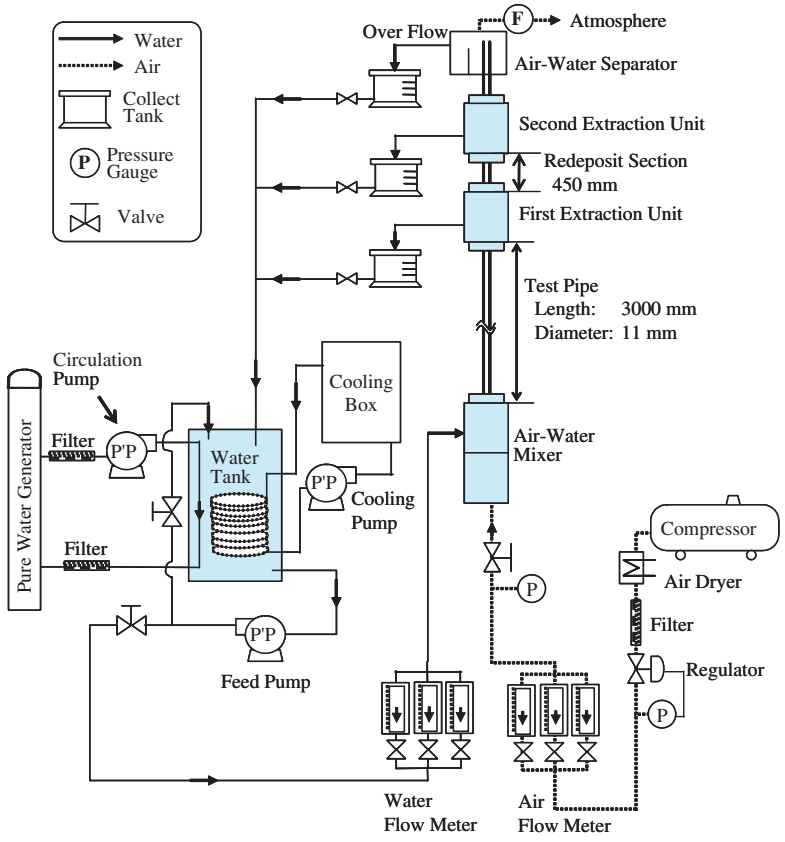

Fig. 3. Annular two-phase flow loop.

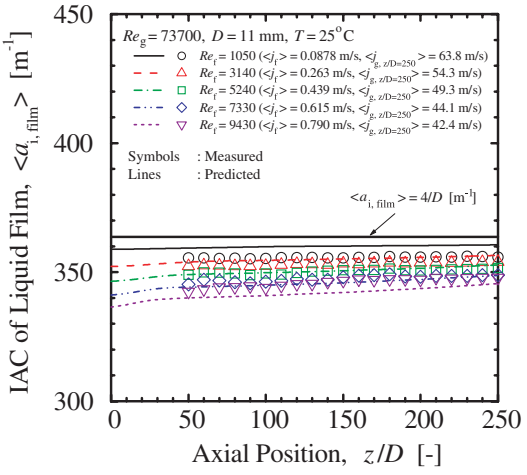

Fig. 4. Axial change of one-dimensional IAC of liquid film ($Re_g = 73{,}700$).

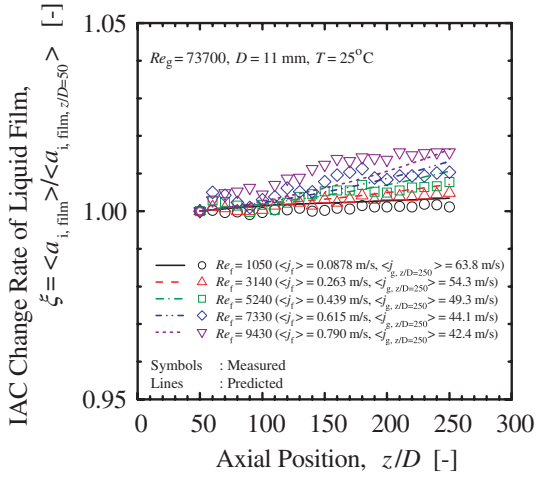

Fig. 5. Rate of one-dimensional interfacial area concentration change ($Re_g = 73{,}700$).

Fig. 4 shows a typical result of the axial development of the one-dimensional interfacial area concentration of the liquid film. Symbols and lines in the figure indicate the measured and predicted values, respectively. In order to highlight the effect of the entry length, the interfacial area concentration normalized by that at $z/D = 50$, $\xi(\equiv \langle a_{i,film}\rangle / \langle a_{i,film,z/D=50}\rangle)$ is also plotted against the axial position as shown in Fig. 5.

As can be seen from Figs. 4 and 5, as the flow develops, the interfacial area concentration of the liquid film gradually increases up to 3% at maximum in the present experimental flow range. The axial increase of the interfacial area concentration of the liquid film is more pronounced at higher liquid Reynolds number, whereas it is insignificant at lower liquid Reynolds number. According to the criterion on the onset of the liquid entrainment, the liquid

droplet entrainment occurs in all the conditions except for $Re_f = 1050$. The liquid droplet entrainment may act as the source for the interfacial area concentration of the liquid film. This can be seen from Eqs. (7) and (19). Eq. (7) indicates α_d increased by increasing E_d, and the first term on the right-hand side of Eq. (19) indicates that the increased α_d increases $\langle a_{i,film} \rangle$. The increased void fraction due to the pressure reduction along the axial direction also tends to increase $\langle a_{i,film} \rangle$. Thus, the axial increase in the interfacial area concentration of the liquid film is mainly due to increase in the liquid droplet entrainment and the void fraction along the flow direction.

In addition, the pressure difference between the inlet and the outlet at high liquid Reynolds number is higher than that at low liquid Reynolds number due to increase in the interfacial shear stress. This causes the increase in the void fraction and the liquid entrainment in axial direction, and results in the pronounced axial increase of interfacial area concentration at higher liquid Reynolds number. The changes of axial interfacial area concentration obtained from measured local liquid film thickness with axisymmetric liquid film thickness assumption are well-reproduced by the existing drift-flux model together with the entrainment rate correlation within an averaged prediction error of ±2.5%.

As shown in Eq. (20), the interfacial area concentration of the liquid film in annular-mist flow is often assumed to be $4/D$. The interfacial area concentration of the liquid film under this assumption is calculated to be 364 m^{-1} in the present test section, see the thick solid line in Fig. 4. The maximum difference between the measured interfacial area concentration of the liquid film and $4/D$ is 7.7% in the present experimental conditions. Thus, as the first assumption, Eq. (20) may be acceptable, but more sophisticated method such as the drift-flux model and the interfacial area transport equation to be developed should be preferable particularly in the critical heat flux prediction.

Figs. 6 and 7 show the dependence of the interfacial area concentration of the liquid film on the gas Reynolds number and the liquid Reynolds number, respectively, at a fixed axial location of $z/D = 250$. As can be seen from Fig. 6, the effect of the gas Reynolds number on the interfacial area concentration of the liquid film at a fixed liquid Reynolds number is more pronounced at higher liquid Reynolds number. The interfacial area concentration of the liquid film at a fixed liquid Reynolds number gradually increases with the gas Reynolds number, see Fig. 6, whereas the interfacial area concentration of the liquid film at a fixed gas Reynolds number decreases with increase of the liquid Reynolds number, see Fig. 7. As the gas Reynolds number increases, the interfacial shear force between the gas core and the liquid film tends to reduce the thickness of the liquid film. The dependences of the interfacial area concentration of the liquid film on the gas and liquid Reynolds numbers are well-reproduced by the existing drift-flux model together with the entrainment rate correlation within an averaged prediction error of ±2.5%.

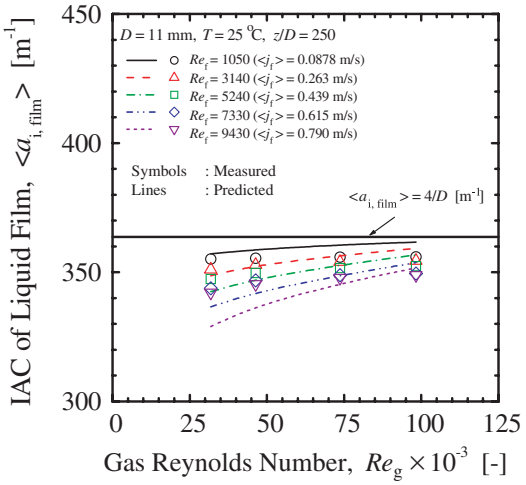

Fig. 6. Effect of gas Reynolds number on one-dimensional IAC of liquid film.

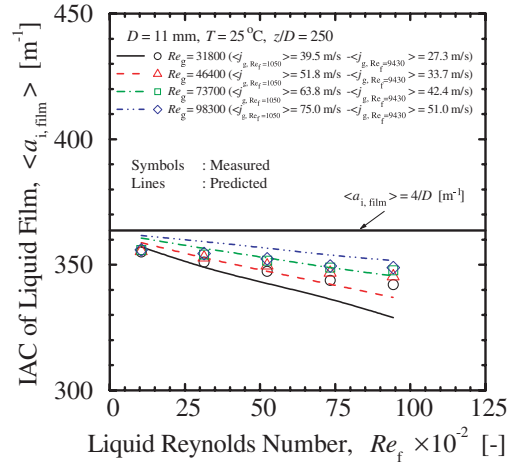

Fig. 7. Effect of liquid Reynolds number on one-dimensional IAC of liquid film.

Fig. 8 shows a typical result of the axial development of the one-dimensional interfacial area concentration. Symbols, thick lines and thin lines in the figure indicate the measured interfacial area concentration of the liquid film, the predicted interfacial area concentration of the liquid film and the predicted total interfacial area concentration of the liquid film and the liquid droplets, respectively. The total interfacial area concentration is estimated by the existing correlations on the liquid droplet size and entrainment ratio (refer to Eqs. (18) and (19) with assuming $C_{an} = 1$, Eqs. (21), (22) and (24)). In order to highlight the interfacial area concentration of the liquid film normalized by the total interfacial area concentration η ($\equiv \langle a_{i,film} \rangle / \langle a_{i,total} \rangle$) is also plotted in Figs. 9 and 10. As can be seen from Fig. 8, no liquid droplet entrainment at the test section inlet occurs at $Re_f = 1050$. However, the acceleration of the liquid film velocity due to the gas expansion initiates the liquid droplet entrainment at a certain

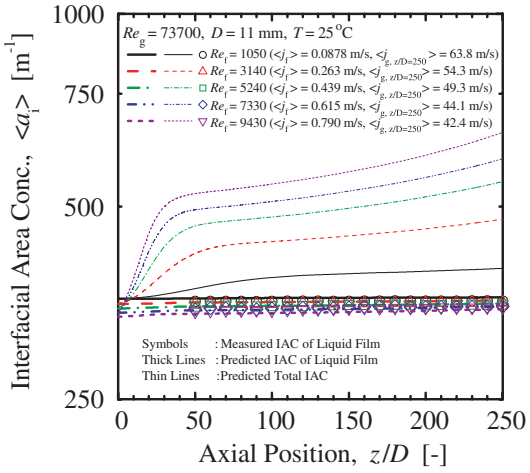

Fig. 8. Axial development of IAC of liquid film and droplet ($Re_g = 73{,}700$).

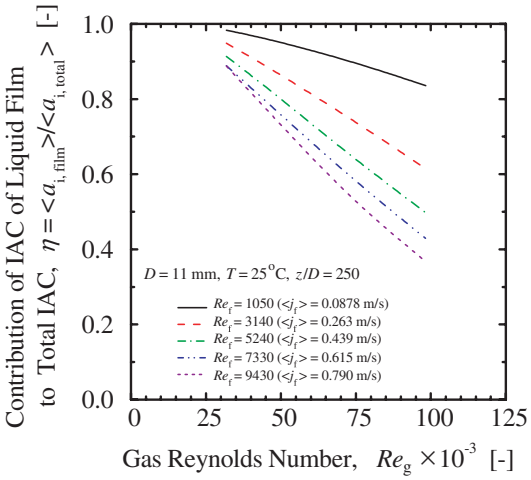

Fig. 9. Contribution of IAC of liquid film to total IAC (effect of gas Reynolds number).

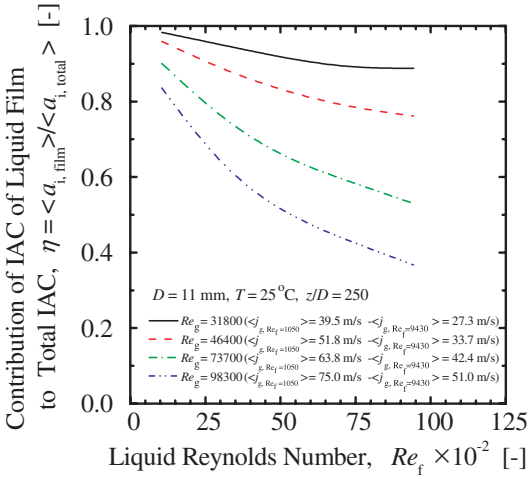

Fig. 10. Contribution of IAC of liquid film to total IAC (effect of liquid Reynolds number).

axial location from the inlet. As the liquid Reynolds number increases, the significant liquid droplet entrainment occurs near the test section inlet resulting in the remarkable increase of the total interfacial area concentration. Such an intensive liquid droplet entrainment appears to be terminated near the test section inlet, and the gradual liquid entrainment occurs at the downstream.

Figs. 9 and 10 show the contribution of the interfacial area concentration of the liquid film to the total interfacial area concentration, η, on the gas and liquid Reynolds numbers. As the gas and liquid Reynolds numbers increase, the contribution of the interfacial area concentration of the liquid film decreases. The contribution, η, is about unity at relatively low gas and liquid Reynolds numbers such as $Re_g = 31{,}800$ and $Re_f = 1050$ due to insignificant liquid droplet entrainment. The contribution, η, is higher than 0.4 even at $Re_g = 98{,}300$ and $Re_f = 9430$. This suggests that the liquid film plays an important role in the interfacial transfer term even at high gas and liquid Reynolds numbers.

4.2. Local interfacial area concentration in liquid film

In this section, local interfacial area concentration of liquid film is examined based on the results of the interfacial waves on a liquid film measured by the LFD. By considering a simple system shown in Fig. 11, where there is only one gas–liquid interface, the position of the interface is represented by

$$x = x_0. \tag{30}$$

Now a control volume, Δx, near the point, γ, is defined by

$$\gamma - \frac{\Delta x}{2} \leqslant x \leqslant \gamma + \frac{\Delta x}{2}. \tag{31}$$

Then, the instantaneous spatial averaged interfacial concentration, a_i, in the control volume, is given by [17]

$$a_{i,film} = \begin{cases} \frac{1}{\Delta x}, & \text{for } |\gamma - x_0| < \frac{\Delta x}{2}, \\ 0, & \text{for } |\gamma - x_0| > \frac{\Delta x}{2}. \end{cases} \tag{32}$$

Here, the instantaneous non-dimensional interfacial area concentration, $\tilde{a}_{i,film}$, is defined by

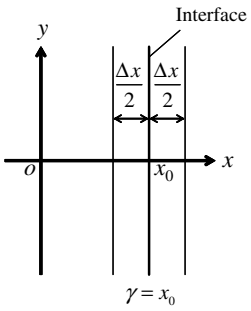

Fig. 11. Definition of local interfacial area concentration in pipe cross section.

$$\tilde{a}_{\mathrm{i,film}} \equiv a_{\mathrm{i,film}}\Delta x = \begin{cases} 1, & \text{for } |\gamma - x_0| < \frac{\Delta x}{2}, \\ 0, & \text{for } |\gamma - x_0| > \frac{\Delta x}{2}. \end{cases} \quad (33)$$

Then, the non-dimensional time-averaged interfacial area concentration, $\overline{\tilde{a}}_{\mathrm{i,film}}$, is expressed by

$$\overline{\tilde{a}}_{\mathrm{i,film}} = \frac{1}{\Delta t}\int \tilde{a}_{\mathrm{i,film}}\,\mathrm{d}t. \quad (34)$$

Thus, the physical meaning of $\overline{\tilde{a}}_{\mathrm{i,film}}$ obtained by this simple model is identical with the fraction of the time period when the interfaces exist within the measuring region of Δx over the total sampling time. The non-dimensional time-averaged interfacial area concentration, $\bar{\tilde{a}}_{\mathrm{i,film}}$, is determined experimentally from the fraction of the time period when the interfaces exist within the measuring region of Δx over the total sampling time. Here, Δx is set at 40 μm.

Fig. 12 shows a typical result of the non-dimensional interfacial area concentration distribution of the liquid film obtained at $z/D = 250$ at a fixed gas Reynolds number of $Re_g = 73{,}700$. Here, $r/R = 1.0$ corresponds to the pipe wall. As shown in the figure, the distribution of the non-dimensional interfacial area concentration of the liquid film is dependent on the flow condition. The distribution has a sharp peak close to the pipe wall at low liquid Reynolds number such as $Re_f = 1050$. As the liquid Reynolds number increases, the peak location tends to shift toward the pipe center, and its amplitude is reduced. This is due to wavy interfacial geometry pronounced by the increased liquid Reynolds number.

Fig. 13 shows a typical result of the axial change of the non-dimensional interfacial area concentration distribution of the liquid film obtained at fixed gas and liquid Reynolds number of $Re_g = 98{,}300$ and $Re_f = 9430$. Comparing the data at $z/D = 50$ with the data at $z/D = 150$ and 250, the interface at $z/D = 50$ appears to be more wavy than that at $z/D = 150$ and 250. However, as the flow develops or the gas velocity increases along the flow direction, the interfacial shear force accelerates the liquid film and increases the liquid droplet entrainment resulting in the thinner liquid film.

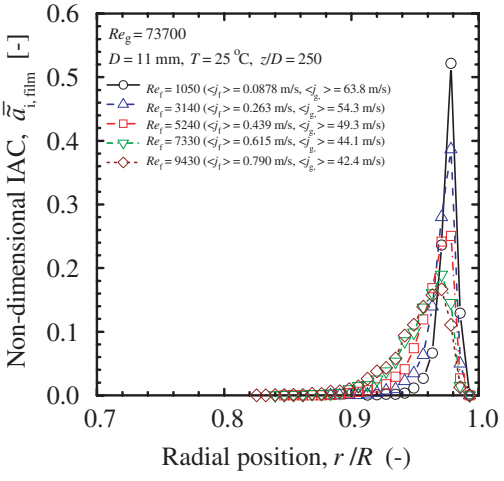

Fig. 12. Effect of liquid Reynolds number on non-dimensional local IAC distribution ($Re_g = 73{,}700$).

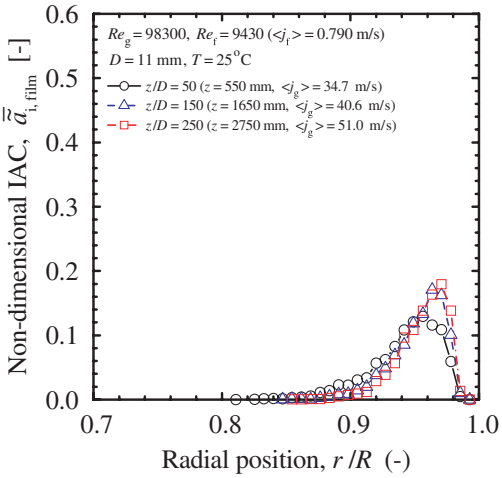

Fig. 13. Effect of liquid entry length on non-dimensional local IAC distribution ($Re_g = 98{,}300$, $Re_f = 9430$).

As the first step to develop the interfacial area transport equation in annular and annular-mist flows, the local and one-dimensional interfacial area concentrations of the liquid film are measured. In order to provide the extensive database enough to evaluate the interfacial area transport equation, the interfacial area concentration of the liquid film together with that of the entrained liquid droplets are necessary. Extensive researches in this direction are encouraged in a future study.

5. Conclusions

As the first step to develop the interfacial area transport equation in annular and annular-mist flows, this study performed the detailed measurement of the axial development of flow parameters such as one-dimensional interfacial area concentration of liquid film and non-dimensional local interfacial area concentration profile of liquid film in vertical air–water flow in 11 mm-diameter pipe in the flow conditions of $31{,}800 \leqslant Re_g \leqslant 98{,}300$ and $1050 \leqslant Re_f \leqslant 9430$. The one-dimensional interfacial area concentration was obtained from the measured local liquid film thickness with the assumption of axisymmetric liquid film, and the non-dimensional time-averaged interfacial area concentration, $\overline{\tilde{a}}_{\mathrm{i,film}}$, was determined experimentally from the fraction of the time period when the interfaces existed within the measuring region of Δx over the total sampling time.

The obtained one-dimensional interfacial area concentration of the liquid film was compared with the drift-flux model by Ishii, and the contribution of the interfacial area concentration in the liquid film to total interfacial area concentration was estimated with help of the drift-flux model

by Ishii, the entrainment correlation by Ishii and Mishima, and the droplet size correlation by Kataoka et al. The obtained results are summarized as follows.

(1) As the flow developed, the pressure reduction along the flow direction gradually reduced the interfacial area concentration of the liquid film up to 3% at maximum in the present experimental flow range.
(2) The axial interfacial area concentration changes were well-reproduced by the existing drift-flux model together with the entrainment rate correlation within an averaged prediction error of ±2.5%.
(3) The simulated calculation showed that the contribution of the interfacial area concentration of the liquid film to the total interfacial area concentration of the liquid film and the entrained liquid droplets was decreased by increasing the gas and liquid Reynolds numbers. The contribution was about unity at relatively low gas and liquid Reynolds numbers of $Re_g = 31{,}800$ and $Re_f = 1050$ due to insignificant liquid droplet entrainment. The contribution was higher than 0.4 even at $Re_g = 98{,}300$ and $Re_f = 9430$. This suggested that the liquid film would play an important role in the interfacial transfer term even at high gas and liquid Reynolds numbers.
(4) The distribution of the interfacial area concentration of the liquid film had a sharp peak close to the pipe wall at low liquid Reynolds number such as $Re_f = 1050$. As the liquid Reynolds number increased, the peak location tended to shift toward the pipe center, and its amplitude was reduced. This was due to wavy interfacial geometry pronounced by the increased liquid Reynolds number.

Acknowledgements

The authors are very thankful to Mr. Y. Fukuhara of Tokyo University of Marine Science and Technology for his collaboration in fabricating the test facilities. Part of this work was performed by the Grant-in-Aid for Scientific Research from Japan Society for the Promotion of Science (Nos. 17560744 and 18760617).

References

[1] G. Kocamustafaogullari, M. Ishii, Foundation of the interfacial area transport equation and its closure relations, Int. J. Heat Mass Transfer 38 (1995) 481–493.
[2] Q. Wu, S. Kim, M. Ishii, S.G. Beus, One-group interfacial area transport in vertical bubbly flow, Int. J. Heat Mass Transfer 41 (1998) 1103–1112.
[3] T. Hibiki, M. Ishii, One-group interfacial area transport of bubbly flows in vertical round tubes, Int. J. Heat Mass Transfer 43 (2000) 2711–2726.
[4] T. Hibiki, M. Ishii, Two-group interfacial area transport equations at bubbly-to-slug flow transition, Nucl. Eng. Des. 202 (2000) 39–76.
[5] T. Hibiki, T. Takamasa, M. Ishii, Interfacial area transport of bubbly flow in a small diameter pipe, J. Nucl. Sci. Technol. 38 (2001) 614–620.
[6] X.Y. Fu, M. Ishii, Two-group interfacial area transport in vertical air–water flow: I. Mechanistic model, Nucl. Eng. Des. 219 (2) (2003) 143–168.
[7] M. Ishii, One-dimensional drift flux model and constitutive equations for relative motion between phases in various two-phase flow regimes, ANL Report 77-47, 1977.
[8] M. Ishii, K. Mishima, Droplet entrainment correlation in annular two-phase flow, Int. J. Heat Mass Transfer 32 (10) (1989) 1835–1846.
[9] I. Kataoka, M. Ishii, K. Mishima, Generation and size distribution of droplet in annular two-phase flow, J. Fluids Sci. 105 (1983) 230–238.
[10] M. Ishii, M.A. Grolmes, Inception criteria for droplet entrainment in two-phase concurrent film flow, AIChE J. 21 (2) (1975) 308–318.
[11] M. Ishii, One-dimensional drift flux modeling: one-dimensional drift velocity of dispersed flow in confined channel, ANL Report 76-49, 1976.
[12] P. Alia, L. Gravarolo, A. Hassid, E. Pedrocchi, Liquid volume fraction in adiabatic two-phase vertical upflow-round conduit, CISE Report 105, 1965.
[13] L. Gravarolo, A. Giorgini, A. Hassid, E. Pedrocchi, A device for the measurement of shear stress on the wall of a conduit: Its application in the mean density determination in two-phase flow: shear stress data in two-phase adiabatic vertical flow, CISE Report 82, 1964.
[14] I. Kataoka, M. Ishii, Mechanism and correlation of droplet entrainment and deposition in annular two-phase flow, ANL Report 82-44, 1982.
[15] T. Takamasa, T. Hazuku, Measuring interfacial waves on film flowing down a vertical plate in the entry region using laser focus displacement meters, Int. J. Heat Mass Transfer 43 (2000) 2807–2819.
[16] T. Takamasa, K. Kobayashi, Measuring interfacial waves on film flowing down tube inner wall using laser focus displacement meter, Int. J. Multiphase Flow 26 (2000) 1493–1507.
[17] I, Kataoka, M. Ishii, A. Serizawa, Local formulation of interfacial area concentration and its measurements in two-phase flow, ANL Report 84-68, 1984.